TURBULENCE AND MODELING IN TRANSONIC FLOW

Morris W. Rubesin and John R. Viegas
NASA Ames Research Center
Moffett Field, California

ABSTRACT

A review is made of the performance of a variety of turbulence models in the evaluation of a particular well-documented transonic flow. This is done to supplement a previous attempt to calibrate and verify transonic airfoil codes by including many more turbulence models than used in the earlier work and applying the calculations to an experiment that did not suffer from uncertainties in angle of attack and was free of wind tunnel interference. It is found from this work, as well as in the earlier study, that the Johnson-King turbulence model is superior for transonic flows over simple aerodynamic surfaces, including moderate separation. It is also shown that some field equation models with wall function boundary conditions can be competitive with it.

INTRODUCTION

The accuracy of aerodynamic computations, at realistic Reynolds numbers where boundary-layer turbulence exists, depends on two distinct, yet interrelated elements. These are the numerical and the physical aspects of the solution scheme. Currently, practical aerodynamic problems have to be solved in a manner where the physical aspects of turbulence, present at the Reynolds numbers of interest, are treated with statistical models. Although such turbulence models can be avoided with time- and space-accurate solutions of the dynamics of turbulence, to date such computations have been confined to very simple flow fields at extremely low Reynolds numbers. Their costs are much too high to be considered for design work in the foreseeable future (ref.1), even if sub-grid models can be developed to allow handling the Reynolds numbers of practical interest.

The statistical equations for turbulent flows, corresponding to the basic Navier-Stokes equations for compressible flows, are derived by first expanding the instantaneous values of the dependent variables, such as velocity components, density, and temperature into the sum of mean and fluctuating quantities. The equations are then either averaged in time, over periods much longer than the time scales of the largest turbulence eddies, or are ensemble-averaged. When transonic flows are considered, simpler equations result when the velocity terms are weighted with the local density in the averaging process. Except for existence or absence of the time-dependent terms, the resulting equations have the same form for either

time- or ensemble-averaging and are called the Reynolds-averaged equations. The dependent variables in these equations are composed of the mean quantities of the velocity and state variables and of moments of their instantaneous quantities. These moments are called Reynolds stresses or heat flux, and it is the evaluation of these quantities that is central to physical turbulence modeling.

In recent years, there has been a considerable expenditure of man-power and computer costs in developing numerical techniques for solving the Reynolds-averaged equations. Today, the flow fields about three-dimensional bodies as complicated as wing-body configurations can be computed in a reasonable time with numerically accurate techniques. The basic algorithms are becoming more efficient and robust, complex meshes are being generated routinely, and codes run sufficiently economically so that mesh-independent solutions can be tested and demonstrated. Color graphics permit detailed and illuminating visualization of the results. Yet despite this enormous rate of progress and maturation of the field of computational fluid dynamics (CFD), the design community still regards the results to be useful only in a qualitative sense and is pressuring the CFD community to calibrate and verify their codes against carefully obtained experimental data so that these codes can be established as accurate design tools.

Because the numerical aspects of a problem can be systematically isolated and improved upon, differences between the output of a good and carefully applied numerical code and experimental data are generally identified as a weakness of the turbulence model. Of course, not all computations are done with the proper care, so that some differences between experimental data and computed results can be numerical as well as physical. That this occurs in published results will be demonstrated by some of the examples shown in the following section.

One attempt to calibrate and verify some existing codes for computing two-dimensional airfoils at transonic speeds was the Viscous Transonic Airfoil Workshop held at the AIAA 25th Aerospace Sciences Meeting at Reno, Nevada, in January 1987, and reported in reference 2. Fifteen different author groups participated, with codes that included 16 Navier-Stokes methods, 2 Euler/boundary-layer methods, and 5 full-potential/boundary-layer methods. The turbulence models variously employed in the Navier-Stokes methods included the classical algebraic eddy viscosity model of Cebeci-Smith (ref. 3), the Baldwin-Lomax algebraic eddy viscosity model (ref. 4), the Johnson-King model (ref. 5), which accounts for turbulence lag with an ordinary differential equation for growth of the maximum shear stress that is then used to scale an algebraic eddy viscosity , and the Coakley q-omega model (ref. 6), the sole representative of the class of two field equation models that define length and velocity scales for an eddy-viscosity evaluation throughout the boundary layer, including the region near the surface. The interactive inviscid-/viscous-layer codes either use the Cebeci-Smith model in the differential equations applying to the boundary layer or an integral model.

The results of this workshop will be summarized in the following section. These results have to be considered to be tentative because they apply to airfoil experiments that experienced wall effects, with an attendant uncertainty in the experimental data, and, also, only a limited number of turbulence models were

represented in the Navier-Stokes computations. To complement this work, a later section of this paper is devoted to the detailed comparison of computed results, from a single computer code that contains a larger number of turbulence models, with the data of an experiment that is relatively free of wind tunnel wall effects and contains measurements of the turbulence itself. These comparisons, as well as the earlier work with the airfoils, are then used here to develop some conclusions regarding the state of the art of modeling turbulence in two-dimensional transonic flows.

SUMMARY OF VISCOUS TRANSONIC AIRFOIL WORKSHOP

The results of the AIAA Viscous Transonic Airfoil Workshop (ref. 2) are summarized on figure 1, where the coefficient of lift is plotted against the coefficient of drag, expressed in counts, for three different airfoils at various Mach numbers and angles of attack. On this figure, the solid circles represent the experimental data. The open circles represent the inviscid/viscous interaction schemes, without distinction as to whether Euler or full potential equations apply to the inviscid region or whether differential or integral methods are used in the boundary layer. The remaining symbols refer to Navier-Stokes calculations. The open squares represent the Baldwin-Lomax algebraic eddy viscosity model; the squares with ticks represent the Cebeci-Smith model; the diamonds represent the Johnson-King lag model, and finally, the triangle represents Coakley's two-equation model.

Figure 1(a) shows the comparison of calculated CL(CD) with the experimental data on an NACA 0012 airfoil (ref. 7) for three conditions of Mach number and angle of attack, all at a chord Reynolds number of nine million. In the lower left-hand corner, there are shown the data and computed results at $M = 0.7$ and at an angle of attack of 1.49°, which includes wind tunnel interference corrections recommended by the experimenter. All of the computed results yield results that are within 10% of the lift, and only two of the inviscid/viscous interactive methods miss the drag by as much as 20 counts. Thus, for attached flows that are weakly transonic, all the computation methods give reasonable quantitative results.

The datum point and computed values of $C_L(C_D)$, at $M = 0.55$ and a corrected angle of attack of 8.34°, are shown in the upper portion of figure 1(a). Under these conditions, the flow over the top of the airfoil had a supersonic bubble followed by a shock wave at about 0.1 chord, where a slight separation occurred. Again, except for two of the viscous/inviscid interactive schemes, the lift is calculated to be between 1% high and 8% low by the various methods. The closest points to the experimental values in terms of C_L and C_D are the Navier-Stokes solutions using the Baldwin-Lomax and Cebeci-Smith models. It is important to note

that equivalent methods, i.e. those solving, ostensibly, the same conservation and modeling equations, also show significant differences, especially in drag. For example, the two Navier-Stokes codes that utilized the Johnson-King model, the diamonds, show differences of over 50 counts in drag coefficient, although lift only differs by about 1%. Similar differences are seen in the results produced by codes employing the Baldwin-Lomax or Cebeci-Smith models. In this example, it is seen that the numerical differences between codes with supposedly the same turbulence models can be larger than the differences produced by the different turbulence models within a single code. These observations bring into serious question the premise stated earlier that code verification processes will be tests primarily of the physical, rather than the numerical aspects of a code. It appears, in this example, that the numerical aspects of some of the codes may have not been treated with sufficient care to make the solutions of each code numerically "correct", thereby permitting their solutions to be differentiated by their physical modeling.

A point that has to be made here is that there are often some arbitrary decisions made in the application of a particular turbulence model, and that some of the differences shown in the last example could be caused by differences in how those decisions were made rather than related to the numerics. For example, in the Cebeci-Smith model, the displacement thickness is used to define the eddy viscosity in the outer region of the boundary layer. The evaluation of a displacement thickness is unambiguous only if the irrotational flow outside the boundary layer produces a uniform velocity component parallel to the surface. This is not the case in the current example and in most complex flows. In fact, this difficulty in defining the displacement thickness was the underlying reason for the changes that were introduced into the Baldwin-Lomax model. This latter model also can suffer from ambiguities, as its velocity scale in the outer regions of the boundary layer can be multivalued. This results in an imprecise prescription of the eddy viscosity in this region. Another significant choice that can introduce differences in the solutions can be the distance of the first mesh point from the surface. If this point does not lie well within the viscous-dominated region of the boundary layer, errors in the skin friction determined by a particular turbulence model can occur. From the published results, it is not possible to discern what differences such choices may have made in the various solutions shown on the figure.

A third example of flow over a NACA 0012 airfoil is shown in the lower right of figure 1(a). Here the Mach number is 0.799 and the corrected angle of attack is 2.26°. Under these conditions, a shock wave developed on the upper surface at about mid-chord that was sufficiently strong to cause significant boundary-layer separation. Again, ostensibly similar methods yield a spread in the results. In this case, however, the two computations with the Johnson-King model agree rather well and, in terms of both C_L and C_D, are the closest to the experimental result, except for the same interactive method that gave the best results in the previous example (ref. 8). In this case the two-equation model gave poorer results than some of the algebraic eddy viscosity models. Also, as in the previous example, most of the codes gave values of drag much larger than the experimental value.

Figure 1(b) shows $C_L(C_D)$ for the RAE 2822 airfoil for two test conditions in reference 9. The symbols have the same meaning as in figure 1(a). Both sets of experimental conditions were obtained at chord Reynolds numbers of $6.5*10^6$. The data point on the left represents the test results at M = 0.725 at a corrected angle of attack equal to 2.92°. A shock wave developed on the upper surface at about X/C = 0.52; but its strength was insufficient to separate the boundary layer. Under these conditions, the bulk of the computational results cluster about the experimental datum point within ±10% on either axis. It is surprising that the computation with the Johnson-King model, the diamond, which was generally the more successful model in figure 1(a), yields one of the poorer results in this case. Here too, the differences between supposedly similar methods show differences as large as those identified with different turbulence models, albeit both sets of differences are relatively small.

The point on the right of this figure corresponds to test conditions at higher Mach number and angle of attack, namely, M = 0.75 and 3.19°. Under these wind tunnel conditions, the upper surface experiences a shock wave, still at X/C = 0.52, but with a strength sufficient to cause boundary-layer separation according to most of the turbulence models. Here the better computed results are due to three viscous/inviscid interactive models, including that of reference 8, and the Johnson-King model in a Navier-Stokes code. The Coakley two-equation model and the eddy viscosity models cluster together at high values of drag.

The third figure of this group, figure 1(c), relates to an experiment (ref. 10) conducted with a supercritical transonic flow airfoil, designated the VA-2, that was developed in West Germany. For this case, the only computed results that exist are from a single code developed by Coakley (ref. 10) which contains the Cebeci-Smith, Johnson-king, and Coakley's q-omega models. In this case, the tests were conducted at a chord Reynolds number of $6*10^6$ and a wind tunnel angle of attack of 1°. The point on the left of the figure represents the datum at M = 0.73, where a shock wave developed at X/C = 0.35. All the models overpredict the lift, and underpredict the drag. As with most of the cases with the other airfoils, the two-equation model gave results essentially identical with those of the Cebeci-Smith model. The Johnson-King model yielded lift within a few percent of the experimental value, but the drag was 30 counts too low, and no better than the values from the other models.

The point on the right of figure 1(c). corresponds to a Mach number of 0.78, where the shock wave moved to X/C = 0.645, rather far back on the airfoil. Again, the lift is predicted well by the Johnson-King model, whereas the other models do much better with regard to drag.

Several conclusions can be drawn from the above discussion of the comparison of calculated $C_L(C_D)$ with the experimental data from three different airfoils in transonic flow. These are as follows:

1. In two-dimensions, some interactive inviscid/viscous methods can be competitive with Navier-Stokes computations containing the better turbulence models.

2. In the Navier-Stokes codes, the algebraic models of Cebeci-Smith and Baldwin-Lomax yield similar results, which are generally equivalent to results from the the more complex Coakley two-equation q-omega model.

3. The Navier-Stokes codes that yield the best results in most of the cases employ the Johnson-King model.

These must be treated as tentative conclusions. Although the data represent the state of the art, they suffer, as do most wind tunnel experiments, from wall interference effects, especially those cases where the airfoils experienced larger regions of separation. A manner of accounting for the wind tunnel effects is to "correct" the geometrical angle of attack to some effective value. In the computations cited above, the effective angles of attack used by the various author groups differed from each other and the reasons for selecting particular values were not stated in reference 2. How much the uncertainty in the angle of attack in each case affects the results shown in reference 2 is not clear. In addition, the assessment in reference 2 suffers from a limited number of turbulence models, and in the case of the two-equation model does not represent the best of that class.

To provide a broader assessment of the state of two-dimensional transonic turbulence modeling, we decided to complement the work described above by computing the flow field of a transonic flow whose data have been shown to be free of wind tunnel interference (ref. 11) and angle of attack uncertainty, and to include additional turbulence models. Since all but one of these models are included in a single Navier-Stokes code, the uncertainties introduced by different codes and solution algorithms are also essentially eliminated. These results are described and discussed in the following section.

TRANSONIC FLOW TURBULENCE MODEL COMPARISONS

Experimental Basis for Comparison

The experiment chosen as the standard for the turbulence model comparisons utilized the transonic flow over a circular arc bump affixed to a hollow circular cylinder aligned with the flow direction (ref. 11). The bump acts aerodynamically in a manner similar to the top surface of an airfoil. The configuration of this wind tunnel model and the flow conditions for which most of the turbulence model comparisons were made are shown on figure 2. The thin-walled cylinder was 15.2 cm in diameter and extended 61 cm upstream of the bump's leading edge. The bump had a chord of 20.32 cm and a thickness of 1.91 cm. At its leading edge, the bump departed from its circular arc shape and blended smoothly into the upstream cylinder. Natural transition occurred on the cylinder, and the resulting turbulent boundary-layer thickness at the leading edge of the bump was about 1 cm. This was sufficiently thick to allow boundary layer measurements, but not so thick as to introduce significant streamwise curvature effects. The measurements included surface pressure, mean velocities, and the Reynolds stresses. These latter data, being profile measurements, allow examination of the reasons for the success or

failures of individual turbulence models. Another decided advantage of using this experiment as a standard is the fact that the wind tunnel model was run in both the NASA Ames Research Center 2 × 2 ft and 6 × 6 ft transonic wind tunnels and that the pressure distributions at the same Mach and Reynolds numbers were essentially the same (ref. 12). This suggests that the data used to test the turbulence models are relatively free of wind tunnel interference. Of course, another advantage of this data set is the lack of ambiguity regarding the angle of attack, as was the case with the airfoils. A shortcoming of using these data, however, is that they were used to develop the Johnson-King model and, therefore, it would be expected that the best performance other models could be made to achieve would be to approach the behavior of this lag model. Therefore, testing a variety of turbulence models with these data can lead to a necessary condition for other turbulence models to satisfy, but is not sufficient for ascertaining the relative performance of turbulence models for flows with separation more massive than occurred within the referenced experiment.

Numerical Procedure

The primary numerical procedure used in computations shown here was originally developed by C. C. Horstman (ref. 13) based on MacCormack's 1981 algorithm (ref. 14). The code has been modified into a series of codes to accommodate the various turbulence models compared in this paper. The MacCormack method used here is basically an explicit second-order, predictor-corrector finite-difference method, modified by an efficient implicit algorithm. In the calculations, the computational domain extended in the flow direction from -140 cm to +90 cm, relative to the onset of the bump. In the radial direction the domain extended from the surface of the model to a radius of 90 cm. The mesh size was 129 × 45, and allowed variable spacing in both the axial and radial directions. In the streamwise direction, the mesh varied from 0.16 cm, near the shock wave, to 12 cm at the downstream boundary. Normal to the surface, an exponentially stretched mesh was used that allowed the first mesh point from the surface to lie well within the sublayer, for those cases where integrations were performed to the surface. When wall functions were used, the near wall mesh centers were generally well into the fully turbulent flow, except at the stations close to and within the separation zone.

The upstream boundary conditions were prescribed by uniform free stream conditions, with the total pressure and temperature held constant and the static properties found from relationships based on the method of characteristics. The downstream conditions set all axial gradients to zero. In all cases, the surface boundary conditions were zero velocity and near adiabatic wall temperature. Uniform free stream conditions were applied at the far-radial boundary, as justified in reference 15.

As discussed in the next section, the Wilcox-Rubesin turbulence model (ref. 16) required a different numerical algorithm, namely MacCormack's 1976 hybrid method, reference 17.

Turbulence Models Considered in Comparative Analysis

In this comparison of turbulence models, the following turbulence models were applied: Cebeci and Smith (ref. 3), Johnson and King (ref. 5), Jones and Launder (ref. 18), Viegas and Rubesin (refs. 19 and 20), Coakley (refs. 6 and 21), and Wilcox and Rubesin (ref. 16). One feature characteristic of all these models is that Reynolds stresses are expressed in terms of an eddy viscosity in a Boussinesq constitutive relationship.

The Cebeci-Smith turbulence model divides the boundary layer into an inner and outer zone, where the eddy viscosity is expressed algebraically in each layer. In the inner layer, the eddy viscosity is expressed with a length scale that is the distance from the surface and and with a velocity scale that is the shear velocity at the wall. In the outer layer these scales are the displacement thickness, computed neglecting density variations, and the boundary-layer edge velocity. The extent of the inner layer is determined by requiring the minimum of the eddy viscosities corresponding to the inner and outer layers be used at each position from the surface. This model has become the standard for use with attached boundary-layer flows. In its current application (ref. 15) the van Driest damping function, used to account for viscous effects in the sublayer and buffer layer, was corrected for non-zero values of the streamwise pressure gradient.

Next in mathematical complexity is the turbulence model of Johnson and King. This model also divides the boundary layer into two zones where the eddy viscosities are expressed algebraically. In the inner layer, however, the velocity scale used in this model depends on the maximum shear stress within the boundary layer, not the wall shear stress (e.g. expressed as shear velocity) as in the Cebeci and Smith model. This maximum shear stress is found from the solution of an ordinary differential equation that represents the rate of the development of the maximum shear stress with distance along the surface. The equation is expressed conveniently in terms of the departure of shear stress and eddy viscosity from their corresponding quantities in equilibrium with the mean motion. Compared to the Cebeci and Smith model, the Johnson and King model contains two additional modeling coefficients, one that scales the rate of development of the maximum shear stress and another that scales the effect of turbulence diffusion within that rate equation. The values of these coefficients were chosen by comparison with the data of reference 18, as well as with those from the bump experiment (ref. 11). The computed results using this model are from reference 5.

The next turbulence model to be discussed is that of Jones and Launder, reference 19. This model is an example of turbulence models that employ two additional partial differential field equations to evaluate the velocity and length scales of the turbulence, thereby allowing for the rate processes in the development in the local state of the scales of turbulence. In this model, the dependent variable in the first equation is the kinetic energy of turbulence, whereas that in the second equation is the rate of dissipation of the turbulence kinetic energy. In establishing the eddy viscosity, the kinetic energy of turbulence acts as the velocity scaling parameter, while the length scale is composed of an algebraic combination of the kinetic energy and the rate of dissipation of kinetic energy. This model also

possesses the feature of special viscous terms in these turbulence field equations that allow integrations to the surface. The model has been extended to account for compressibility, necessary in the computation of transonic flows, by use of mass weighting the turbulence equations and allowing for non-zero mean velocity divergence in the constitutive relationship for the eddy viscosity.

It has been shown that the popular Jones-Launder turbulence model yields poor values of skin friction in the presence of a shock wave in transonic flow, and that the introduction of wall functions, originally designed to save computation costs, surprisingly improved the prediction of skin friction (ref. 20). Accordingly, the compressible-flow, wall-function models of Viegas and Rubesin were applied to the Jones-Launder model for the test case considered here. These wall-function approaches allowed use of fewer mesh points normal to the surface and reduced the stiffness of the turbulence equations; both effects lead to considerable saving in computation costs over that of the Jones-Launder model itself.

These wall-function methods depend on establishing the wall shear from a knowledge of the mean velocity at the center of the first mesh volume off the surface and from the turbulence kinetic energy at the centers of the first two points off the surface. The latter kinetic energy information reflects the local axial pressure gradient along the surface. In addition, these wall-function methods rely on careful integrations of the production and dissipation of the kinetic energy across the first mesh volume in order to have the mean kinetic energy identified with the mesh volume reflect the presence of the sublayer and buffer layers that exist there. In the first of the wall function methods (ref. 20), the "law of the wall" was used with fixed coefficients appropriate strictly for flat plates at constant pressure. In the second wall function method (ref. 21), these coefficients were allowed to vary, reflecting the behavior of the sublayer to strong axial pressure gradients, and in addition, provisions were made for the presence of the lower portion of the wake region of the boundary layer. These modifications are influential only in regions approaching separation, and in the separation zone, and immediately after reattachment. It should be noted that it was the added viscous terms (the so-called "low Reynolds number terms") which allowed integrations to the surface in the Jones Launder model that caused its difficulties and were eliminated through the use of the wall function approaches.

Another turbulence model used in these comparisons was that of Wilcox and Rubesin (ref. 16). This model is similar to that of Jones and Launder in that two turbulence field equations also are employed to yield turbulence scale quantities on which to base the eddy viscosity. In this model, the variable used to develop the length scale is the specific rate of dissipation, i.e. the rate of dissipation divided by the kinetic energy. The turbulence model differs from the Jones-Launder model in another very significant way; it does not require additional viscous terms to permit integrations to the surface, but accomplishes this through the use of damped coefficients in the high Reynolds number terms. A drawback of this turbulence model is that the second equation uses the square of the specific dissipation rate as its dependent variable. This is a quantity that varies with distance from the surface to the fourth power, a variation that is too rapid for the second-order

finite differencing used in the computations to be accurate in the vicinity of the surface. To avoid inaccuracies, very near the surface an analytical expression is used to evaluate the dissipation rate variable. This analytical expression, however, causes instabilities at the match point with the numerical solution of the second modeling equation. In addition, this model has particularly stiff mathematical characteristics when wall functions are not used. These instabilities and stiffness characteristics prevented this model from being incorporated into the same algorithm as was used for all the other turbulence models (ref. 20). Consequently, the results presented here for the model of Wilcox and Rubesin were obtained with the older, less efficient, more complicated, but more robust hybrid code of MacCormack (ref. 17). The results of this model shown here are restricted to the surface pressure distribution, the only recoverable results available to the authors (ref. 15).

To relieve the near-surface numerical difficulties associated with the Wilcox-Rubesin model, Coakley (refs. 6 and 22) developed turbulence models in which the dependent variables of the turbulence field equations were the slower varying square root of the kinetic energy and the first power of the specific dissipation rate. Coakley introduced low Reynolds number and damping terms that reduced or eliminated the types of unusual stiffness associated with the Wilcox-Rubesin and the Jones-Launder turbulence models and allowed efficient computation. In defining the coefficients of these new equations, Coakley transformed those of Jones and Launder into what is called here "Coakley-1" and those of Wilcox and Rubesin into "Coakley-2". Recall that the airfoil computations shown earlier were based on the Coakley-1 turbulence model.

Results of Turbulence Model Comparison

Figures 3(a) and 3(b) show the comparison of computed results based on the variety of turbulence models with the experimental surface-pressure data obtained in reference 11. The figures display the pressure coefficient distribution over the downstream half of the bump followed by one-half chord length of the cylinder. On these figures the experimental data, corresponding to a Mach number of 0.875 and a Reynolds number of $13.1 \times x10^6$, are represented by the open circles, whereas the computed results are indicated with solid lines. The same data points are common to all the figures. Figure 3(a) compares the turbulence models of Cebeci-Smith, Johnson and King, and Coakley's two versions of the two equation model. As expected, the Johnson-King model produces excellent results, in both locating the position of the shock wave and representing the pressure levels in the region of separation (see table 1). On the other hand, use of the classic Cebeci-Smith turbulence model yields a shock-wave location that is about 1/10th chord downstream from the experimental value, and much higher pressures in the region of separation. The results based on the use of the Coakley-1 model are quite similar to those of the Cebeci-Smith model. This behavior illustrates why Coakley's higher-order model results in the airfoil calculations shown in figure 1 were so similar to those from the Cebeci-Smith or Baldwin-Lomax algebraic models. The modified model, Coakley-2, shows some improvement in establishing both the location of the shock wave and in

the pressure level in the vicinity of separation. Figure 3(b) shows the same curves for the turbulence models of Jones-Launder, Wilcox-Rubesin, and three-examples of the Viegas-Rubesin wall function methods as applied to the Jones-Launder model. It is observed that the Jones-Launder model yields results quite similar to those of Coakley-2, with a slightly better prediction of the shock location but with essentially the same pressures in the separation zone. The other two-equation model, Wilcox-Rubesin, shows pressure coefficients that are uniformly lower than the others. These latter results are from computations made with the older hybrid code in which upstream boundary conditions were not consistent with requirements along characteristic lines as is made in the more modern codes. If the computed results from the Wilcox-Rubesin model are moved downward, i. e. the C_p are lowered uniformly, they agree essentially with those from Jones-Launder or Coakley-2. These comparisons reveal that the two-equation turbulence models, except for Coakley-1, yield about the same pressure-distribution results regardless of dependent variable used in the second scale equation or of the differences in the details of how the equations are modified to permit integration to the surface.

The remaining figures on figure 3(b) demonstrate the results from computations employing the wall-function techniques of references 20 and 21 with the Jones-Launder turbulence model. These techniques can reduce computation costs by about an order of magnitude (ref. 20). In these cases, the slightly low values of C_p shown ahead of the shock wave are believed to be caused by use of slightly high value of free-stream dynamic pressure. The basis of this observation is that comparisons directly in pressure show better agreement.

The figure on the lower right represents the results from the simpler wall function version, reference 20. Two curves are presented, representing the results corresponding to different sizes of the initial mesh volumes adjacent to the surfaces. These are identified by the value of y^+, the dimensionless wall distance corresponding to the center of the mesh volume and values of the wall shear stress about a chord upstream of the bump's leading edge. Because an exponential version of the logarithmic "law of the wall" is used to define surface shear in this wall-function technique, it is desirable to assure that the y^+ lies well within the fully turbulent flow, that is, to have a value greater than about 30. Accordingly, two values of y^+ were tried, namely $y^+ = 140$ and $y^+ = 60$. It is observed that the computed location of the shock wave is sensitive to the choice of the y^+. The pressure level in the separation zone, however, is not as sensitive to the different y^+. The case with $y^+ = 60$ gives results that are a decided improvement over those from the original Jones-Launder model. For this wall-function scheme, it appears that the size of the first mesh cell adjacent to the surface becomes another modeling decision, or constant, in the process. Partially to remedy this matter, the second wall-function scheme was developed in reference 21. While reducing the sensitivity of the results to the value of y^+, the effect was not entirely eliminated and the y^+ still remains a modeling parameter. The results with $y^+ \square 140$ and the improved wall-function technique are shown in the lower-left of the figure. These results are very good in establishing both the location of the shock wave and pressure levels in the region of separation, and are the nearest rival to the Johnson-King model. With $y^+ = 60$, for this wall-function model, values of

pressure coefficient indicated a movement of the predicted location of the shock wave of $x/c = 0.02$ from the $y^+ = 140$ case, and otherwise acted similarly to the $y^+ = 60$ case of wall function 1. The $y^+ = 60$ case with the wall function 2 model also showed some waviness in the pressure coefficient in the separated zone that we believe was caused by the absence of a buffer region in this model.

When the values of skin friction evaluated by the various models are compared, it is found that they differ to a very large extent. Unfortunately, no measurements of skin friction were made in the experiment of reference 11 so that no conclusions regarding the relative merit of the the various turbulence models regarding skin friction can be made. The experiment did contain measurements of the mean points of separation and reattachment obtained by means of the oil film technique. These data and the points that bound the regions in the computations where skin friction is negative (i.e., the separation zone) are indicated in table 1. Again, the superiority of the Johnson-King model is demonstrated as it almost duplicates the experimental data. The wall-function techniques with chosen values of y^+ are next in performance, showing reattachment locations on the cylinder roughly 0.1 of the bump's chord upstream of the measured location. Finally, all of the two-equation models with integration to the surface show separation points approximately 0.3 chord downstream of the measured values and reattachment points about 0.1 chord upstream.

Figure 4 shows the development of the displacement thickness over the rear half of the bump and on the downstream cylinder. Recall that it is the displacement thickness that produces the influence of the viscous region upon the inviscid flow. As in figure 3, the experimental data are shown with open circles and are repeated on each of the graphs to facilitate the comparison of the various models. In figure 4(a), it is seen that the classic Cebeci-Smith model gives results that are quite inferior to the Johnson-King model. The Coakley-1 model, in this case, performs a bit better than does the Cebeci-Smith model, and the improvements in Coakley-2 are quite significant in the region of rising displacement thickness. In figure 4(b), the Jones-Launder model is shown again to yield results essentially the same as those of Coakley-2. The Viegas-Rubesin wall-function-1 approach with $y^+ = 140$ produces similar results. The other wall-function approaches, with their selected values of y^+, yield results for displacement thickness that surprisingly are even better than those of the Johnson-King model.

Another interesting variable with which to compare the performance of the various turbulence models is the the shape factor. It is a quantity that enters the momentum integral equation used in some of the inviscid-viscous interactive schemes, and also can be used to infer the behavior of the momentum thickness, since all of the turbulence models yielded reasonably accurate values of the displacement thickness. Figure 5 shows the development of the shape factor over the latter half of the bump and on the downstream cylinder. One feature evident from all the computed results is a dip in the shape factor at the onset of separation, something that is not evident in the experimental data. The cause of this is unknown. Other than this, it is seen in figure 5(a) that the shape factor given by the Johnson-King model generally behaves the best of the models. The Cebeci-Smith and the Coakley-1

models fail to develop the steep rise in the shape factor evident in the data in the separation region. This is evidence that the momentum integral computed by these models in this region must be much higher than the actual. This behavior is corrected to some extent by the Coakley-2 model and the Jones-Launder model shown in figure 5(b) The wall function models give mixed results. The case of the Viegas-Rubesin wall function 1 with $y^+ = 60$, which gave the better results for the other variables considered previously than did the case with $y^+ = 140$, overshoots the data in the region just aft of the point of separation. This shows that the local momentum thickness computed with $y^+ = 60$ must be yielding low values of the momentum thickness there. The Viegas-Rubesin wall-function-2 computation with $y^+ = 140$ shows similar tendencies but behaves quite well over the downstream cylinder. The irregularities shown in this latter figure are believed to be the result of locally low values of the y^+ in the region of separation. This can allow the center of the first mesh volume off the surface to be either within a fully turbulent and/or fully laminar zone of the boundary layer (one of the features that is permitted by this version of the wall function models). Blending these distinct layers with a buffer layer could possibly have avoided the bumps and valleys of the computation.

To further illustrate the relative behavior of the various turbulence models, the velocities in the axial direction predicted by the computations are compared in figure 6 with the corresponding measured data. All the profiles are at stations within the experimentally determined separation zone over the trailing-edge region of the bump and the cylinder downstream. The velocities are normalized by the free-stream velocity and plotted as functions of the vertical distance from the surface expressed in centimeters. With linear coordinates, a plot such as this only shows the behavior of what is usually termed the outer portion of the boundary layer. The sublayer and buffer layer cannot be seen distinctly without recourse to logarithmic plotting. These profiles are shown at values of $x/c = 0.75$, 0.875, 1.00 (the trailing edge of the bump), and 1.125. Recall that separation and reattachment was indicated at $x/c = 0.67$ and 1.17. At $x/c = 0.75$, roughly 1/10th chord downstream of the mean separation, it is surprising that the Johnson-King model does not show the best agreement with the velocity data in view of its success in predicting the surface pressure and integral thicknesses. A possible explanation of this behavior is given in reference 12 where it is shown that better agreement between the velocity computations and the experimental data can be achieved by shifting the computed results downstream by only about 0.03 chord. Another way of arguing this point is to note that at $x/c = 0.75$ very rapid changes to the flow field are occurring so that small misalignments between the computations and the experimental data in the streamwise direction cause large apparent profile errors. Subject to this observation as a caveat, it is found that the Coakley-2 and Jones-Launder models give the best fits to the velocity data at this station. Since the flows for these latter models have not yet separated at this station, their agreement with the far field velocity data shows how sensitive near-wall turbulence modeling is to the prediction of surface phenomena. Again, there are similarities in the results of the Cebeci-Smith and Coakley-1 models, and in the wall-function models 1 and 2 with $y^+ = 60$ and 140, respectively. Errors in the velocities toward the outer part of the boundary layer are indications of poor representation of the surface pressure at a particular station, and indicate the largest errors for the

Cebeci-Smith and Coakley-1 models. This observation is consistent with the pressure coefficient results shown on figure 3(a) at $x/c = 0.75$.

The remaining velocity profiles are at stations where flow-field changes are less rapid, and are more indicative of the performance of the various turbulence models. Except for the Cebeci-Smith and Coakley-1 models, all the turbulence models give results for the velocity profiles that are very representative of the experimental data. Apparently, far-field velocity data in and near a region of separation are not critically sensitive to turbulence models employed. Of course, in the near-wall region, this is not the case as the skin friction demonstrated by the various models differed considerably in magnitude and even in sign at some stations. Also, the position of separation is sensitive to the near-wall velocity behavior, and also differed considerably with the different turbulence models.

A final comparison of the performance of the various models is shown in figure 7, where profiles of the Reynolds shear stress parallel to the streamwise direction are compared with the corresponding experimental measurements. Recall that a linear plot in distance from the surface shows principally the behavior of the outer part of the boundary layer. The stations shown cover the experimental region of separation and are the same as those used for the mean velocities in figure 6.

The most striking feature of the series of plots on figure 7 is the similarity of the general behavior all the turbulence models. This behavior is rather surprising when consideration is given to fact that the zones of separation predicted by many of the models had little relationship to the experimental zone covered by these figures. For example, the Coakley-1 model barely shows any separation, yet the Reynolds stresses predicted by it are not that grossly different from those of the Johnson-King model. From this it can be inferred that the Reynolds stresses outside the viscous sublayer and buffer region are rather insensitive to the presence or absence of separation. This observation is consistent with the concept in the algebraic eddy viscosity models that the the proper scaling in the outer part of the boundary layer is the displacement thickness and the velocity at the boundary layer edge, which are more similar in the computations based on the various models than are their zones of separation.

In detail, it is observed that none of the models yields values of Reynolds shear stress as large at the measured values at the downstream stations. The Cebeci-Smith and Coakley-1 models perform the poorest in this regard. The more successful models, however, are those whose peaks of shear stress are larger in magnitude and occur closer to the distances from the surface shown by the maxima in the experimental data. Modeling the outer region of the boundary layer seems to be important in this flow, and may explain why models that account for the out of equilibrium conditions there, through a lag equation or field equations, are the more successful.

CONCLUDING REMARKS

It is generally accepted that there is no unique way of modeling turbulence in transonic flow fields. Consequently, a model can only be gauged by its degree of success in computing a particular type of flow field. To do this, it is necessary to eliminate, as much as it is possible to do so, experimental errors in the data used for model assessment. We tried to do this here by dealing with a two-dimensional flow field that was free of uncertainties due to wind tunnel wall effects and to unknown angles of attack, in contrast to the ambiguities that exist in the current crop of airfoil experiments that were used to assess computation codes and turbulence models earlier. Also, past assessments dealt only with a limited number of turbulence models; two algebraic eddy viscosity models, a lag model that determines the growth of the maximum shear stress along a surface that is then used to scale an algebraic eddy viscosity across the boundary layer, and a single version of two-equation modeling where the variables upon which an eddy viscosity is evaluated are found from field equations. In the present paper, five more two-equation eddy viscosity models have been considered, two of which involve the use of wall functions to represent surface boundary conditions and avoid carrying integration to the surface.

The preceding descriptions of the comparative performance of these turbulence models reflect the two main underlying turbulence modeling philosophies. One approach argues that for a specific class of flows it is best to begin with a simple model and adapt it just enough to capture the most essential elements of the new flow. The other approach is to apply a so-called "universal" model. These employ field equations for their basic variables and can be applied without change to any type of flow. In principle, a good version of the latter type of model would yield accurate quantitative results for a disparate variety of flows. In practice, however, it is found that while the models can be applied rather easily computationally to new situations, the results they give in particular cases are often not as accurate as would be desired for aerodynamic design purposes.

The Johnson-King model is representative of the first approach applied to the development of an accurate model for the prediction of transonic flows over simple aerodynamic bodies. A key element in its development was the recognition that it was essential to account for the nonequilibrium between the turbulence and mean flow in the outer portions of the viscous layers. In contrast, the earlier models of Cebeci-Smith and Baldwin-Lomax assume complete equilibrium between the turbulence and the mean motion. Johnson and King introduced nonequilibrium in the streamwise direction by utilizing an equation to evaluate the rate of development of the maximum shear stress in the boundary layer. This maximum shear stress was then used to scale the eddy viscosity in algebraic expressions across the boundary layer. This latter step implies an equilibrium in the direction normal to the surface. The model required the introduction of two additional modeling constants beyond those used in the algebraic eddy viscosity models. As was shown earlier, this Johnson-King model could be adjusted to produce excellent results for the mean velocities and surface pressures over the axisymmetric bump. This is not surprising as these

experimental data were used to define the additional modeling constants used in the model. Significantly, however, it was found that this model gave good comparisons with low-speed data (ref. 23) and also, as was demonstrated earlier, generally produced the best comparisons among the Navier-Stokes methods with the three sets of independent airfoil data. This suggests that the Johnson-King model has the breadth to be applied with confidence in a predictive sense to some new transonic flow provided it has separation zones comparable in size to those in the flow over the transonic bump.

Several examples were shown of the performance of "universal" two-equation eddy viscosity models integrable to the surface (refs. 6, 19, and 22). These models utilized coefficients that were based on flows in pipes or attached boundary layers, and were unmodified to reflect the requirements of transonic flows with shock waves. Although these models allow the turbulence and mean motion to be out of equilibrium in both the streamwise and normal directions, it was found that the Coakley-1 model gave essentially the same overall results as the equilibrium model of Cebeci-Smith. Note that computations of the transonic flow over the bump have not been made with the Baldwin-Lomax model, but, based on past modeling experience (ref. 2) this model is expected to yield results similar to those of the Cebeci-Smith model. Some improvement occurred with the Coakley-2 model, where the modeling coefficients were altered from those of Coakley-1, but the results were no better than given by the earlier Jones-Launder model. It is not clear why the Coakley-2 model, designed to account more accurately for separated flows at supersonic speeds, did not give more accurate results for the transonic flow considered here. Perhaps the level of effort of trying to improve the Coakley-1 model was less than was exerted by Johnson and King; or the act of improving the field equation models is just inherently more difficult than with the simpler models. In either case, the Coakley-2 model still leaves something to be desired in the prediction of transonic flows.

The other models shown were applications of the use of wall functions to the Jones-Launder model. Implicit in the use of wall functions is the assumption that the near-wall region is one where equilibrium between turbulence and mean flow exists. These wall functions were developed principally to save computer effort by reducing the numerical stiffness and the number of mesh points employed. They have not been tailored for any particular flow or two-equation turbulence model and are quite general. The wall functions have been adapted to three two-equation models of turbulence (two k,epsilon models and the Wilcox-Rubesin model) and successfully applied to a variety of complex flows and over a range of Mach numbers. Generally, the wall functions have made the computer codes more robust and, with a judicious choice of the size of the first mesh volume, can obtain enhanced agreement between the numerical results and the experimental measurements. Such improvements had previously been observed in several transonic duct flow calulations (refs. 20 and 21). Their use here, with dimensions of the first mesh volume that resulted in values of $y^+ = 60$ and 140 for Viegas-Rubesin wall functions methods 1 and 2, respectively, also reduced computation costs and improved the comparison of the computations with the experimental results of the transonic bump flow. It should be noted that these wall functions were of the type that perform accurate integrations

of the production and dissipation of the turbulence kinetic energy within the first mesh volume off the surface. This allows accounting for the larger fraction of the viscous-flow region compared to fully turbulent flow region within this mesh volume that occurs at the stations in or near the separated flow.

It can be concluded from this review that algebraic eddy viscosity turbulence models that assume complete equilibrium between the turbulence and the mean motion, when coupled with the Navier-Stokes equations, are inadequate to yield the accuracies in the calculation of transonic flows that are necessary for aerodynamic design. Based on comparisons with airfoil data and over an axisymmetric bump, it has been found that the Johnson-King model remedied this situation in two dimensional flows by merely adding the complexity of an additional ordinary differential equation to account for the non-equilibrium growth of the maximum shear stress in the boundary layer along the surface. Equilibrium of the turbulence and mean flow is still assumed across the boundary layer. Of course, if an airfoil design contains a surface jet, or multiple control surfaces, situations can develop within the boundary layer where more than one maximum in shear stress can occur and ambiguity in the model develops. Also, the extension of the concept of basing algebraic eddy viscosities on a maximum shear stress to three-dimensional flows will require considerable development and loss of simplicity.

Two-equation models that can be integrated to the surface require further careful development before they can be considered to be predictive models. Emphasis in this development should be on the improvement of performance in the near-wall regions under severe adverse streamwise pressure gradients and in regions of separation. The effort to do this is worthwhile because of the particular adaptability of this class of closure models to new situations. Some examples of this are: three-dimensionality, surface jets, and multi-element airfoils and wings. In design computations involving many changes of parameters, the cost savings introduced by wall functions should not be overlooked. Thus, wall functions should be improved to further reduce the sensitivity of the results to differences in the dimensions of the first mesh volume off the surface.

It is also significant that, to date, some of innovations to turbulence modeling that have shown some promise in low-speed, incompressible flows have not been applied yet to transonic flows. One example of this is the algebraic stress model that eliminates the controversial eddy viscosity constitutive relationship (ref. 24). This approach has inherent advantages when isotropies in the Reynolds stresses are expected to depart from those associated with two-dimensional shear flows. Examples of situations where this is likely to happen are three-dimensional flows, regions of intense streamwise curvature, and in the presence of shock waves. Another example of developments in incompressible flow computations is the four-equation approach, where the shear stress, the most important Reynolds stress, is determined through an additional field equation and the different roles played by the large and small eddies of turbulence, which primarily exchange momentum and dissipate turbulence, respectively are introduced through another kinetic energy equation (ref. 25). In addition, it has been shown that modeling which represents each Reynolds stress with a field equation and utilizes a single-scale equation can

be applied at acceptable computer costs to transonic flows (ref. 26), and fine-tuning of this approach to improve its accuracy is warranted not necessarily as a design tool, but as a standard of comparison and guide for the simpler approaches. Finally, in view of the success of some of the interactive inviscid/viscous methods in predicting the airfoil lift and drag coefficients of figure 1, it would be interesting to see these methods applied to the transonic bump flow and to compare the results to those presented here that were based on solutions to the Reynolds-averaged Navier-Stokes equations.

REFERENCES

1. Rubesin, M. W.: Turbulence Modeling. Supercomputing in Aerospace, NASA CP 2454, 1987.

2. Holst, T. L.: Viscous Transonic Airfoil Workshop Compendium of Results. AIAA Paper No. 87-1460, June 1987.

3. Cebeci, T. and Smith, A. M. O.: Analysis of Turbulent Boundary Layers. Academic Press, 1974.

4. Baldwin, B. S. and Lomax, H.: Thin-Layer Approximation and Algebraic Model for Separated Turbulent Flows. AIAA Paper 78-257, Jan. 1978.

5. Johnson, D. A. and King, L. S.: A Mathematically Simple Turbulence Closure Model for Attached and Separated Turbulent Boundary Layers. AIAA Journal, Vol. 23, Nov. 1985, pp. 1684-1692.

6. Coakley, T. J.: Turbulence Modeling Methods for the Compressible Navier-Stokes Equations. AIAA Paper No. 83-1693, July 1983.

7. Harris, C. D.: Two-Dimensional Aerodynamic Characteristics of the NACA 0012 Airfoil in the Langley 8-Foot Transonic Pressure Tunnel. NASA TM 81927, 1981.

8. Drela, M. and Giles, M. B.: Viscous-Inviscid Analysis of Transonic and Low Reynolds Number Airfoils. AIAA Paper No. 87-0424, Jan. 1987.

9. Cook, P. H., McDonald, M. A., and Firmin, M. C. P.: Aerofoil RAE 2822-Pressure Distributions, and Boundary Layer and Wake Measurements. AGARD-AR-138, 1979.

10. Mateer, G. G., Seegmiller, H. L., Coakley, T. J., Hand, L. A., and Szodruch, J.: An Experimental Investigation of a Supercritical Airfoil at Transonic Speeds. AIAA Paper No. 87-1241, June 1987.

11. Bachalo, W. D. and Johnson, D. A.: Transonic, Turbulent Boundary Layer Separation Generated on an Axisymmetric Flow Model. AIAA Journal, Vol. 24, No. 3, March 1986, pp. 437-443.

12. Johnson, D. A.: Transonic Separated Flow Predictions with an Eddy-Viscosity/ Reynolds-Stress Closure Model. AIAA Journal, Vol. 25, No. 2, February 1987, page 252.

13. Johnson, D. A., Horstman, C. C., and Bachalo, W. D.: Comparison Between Experiment and Prediction for a Transonic Turbulent Separated Flow. AIAA Journal, Vol. 20, No. 6, June 1982, pp. 737-744.

14. MacCormack, R. W.: A Numerical Method for Solving the Equations of Compressible Flow. AIAA Journal, Vol. 20, Sept. 1982, pp. 1275-1281.

15. Horstman, C. C. and Johnson, D. A.: Prediction of Transonic Separated Flows. AIAA Journal, Vol. 22, No. 7, July 1984, page 1001.

16. Wilcox, D. C. and Rubesin, M. W.: Progress in Turbulence Modeling for Complex Flow Fields Including the Effects of Compressibility. NASA TP 517, April 1980.

17. MacCormack, R. W.: An Efficient Numerical Method for Solving the Time-Dependent Compressible Navier-Stokes Equations at High Reynolds Number. Computing in Applied Mechanics, AMD Vol. 18, The American Society of Mechanical Engineers, 1976; also NASA TM X-73,129, 1976.

18. Jones, W. P. and Launder, B. E.: The Prediction of Laminarization with a Two-Equation Model of Turbulence. International Developments in Heat Transfer, Vol. 15, 1972, pp. 303-314.

19. Viegas, J. R., and Rubesin, M. W.: Wall-Function Boundary Conditions in the Solution of the Navier-Stokes Equations for Complex Compressible Flows. AIAA Paper No. 83-1694, July 1983.

20. Viegas, J. R., Rubesin, M. W. and Horstman, C. C.: On the Use of Wall Functions as Boundary Conditions for Two-Dimensional Separated Compressible Flows. AIAA Paper No.85-0180, Jan. 1985.

21. Vuong, S. T. and Coakley, T. J.: Modeling of Turbulence for Hypersonic Flows With and Without Separation. AIAA Paper No. 87-0286, Jan. 1987.

22. Simpson, R. L., Chew, Y. T., and Shivaprasad, B. G.: The Structure of a Separating Turbulent Boundary Layer, Part 1: Mean Flow and Reynolds Stresses. Journal of Fluid Mechanics, Vol. 113, April 1983, pp. 23-51.

23. Sindir, M. M. S.: Numerical Study of Turbulent Flows in Backward-Facing Step Geometries: Comparison of Four Models of Turbulence. Ph.D. Dissertation, University of California, Davis, 1982.

24. Wilcox, D. C.: Multiscale Model for Turbulent Flows. AIAA Paper No. 86-0029, Jan. 1986.

25. HaMinh, H., Rubesin, M. W., Vandromme, D., and Viegas, J. R.: On the Use of Second Order Closure Modelling for the Prediction of Turbulent Boundary Layer/Shock Wave Interactions: Physical and Numerical Aspects. International Symposium on Computational Fluid Dynamics, Tokyo, Japan, Sept. 9-12, 1985.

TABLE 1.- LOCATION OF SEPARATION AND REATTACHMENT, x/c

	Separation Point	Reattachment Point
Experiment	0.67	1.17
Cebeci-Smith	0.73	1.04
Johnson-King	0.68	1.17
Coakley 1	0.99	1.00
Coakley 2	0.96	1.04
Jones-Launder	0.94	1.04
Viegas-Rubesin Wall Function 1		
$y^+ = 60.0$	0.68	1.08
$y^+ = 140.0$	0.85	1.06
Viegas-Rubesin Wall Function 2		
$y^+ = 140.0$	0.69	1.11

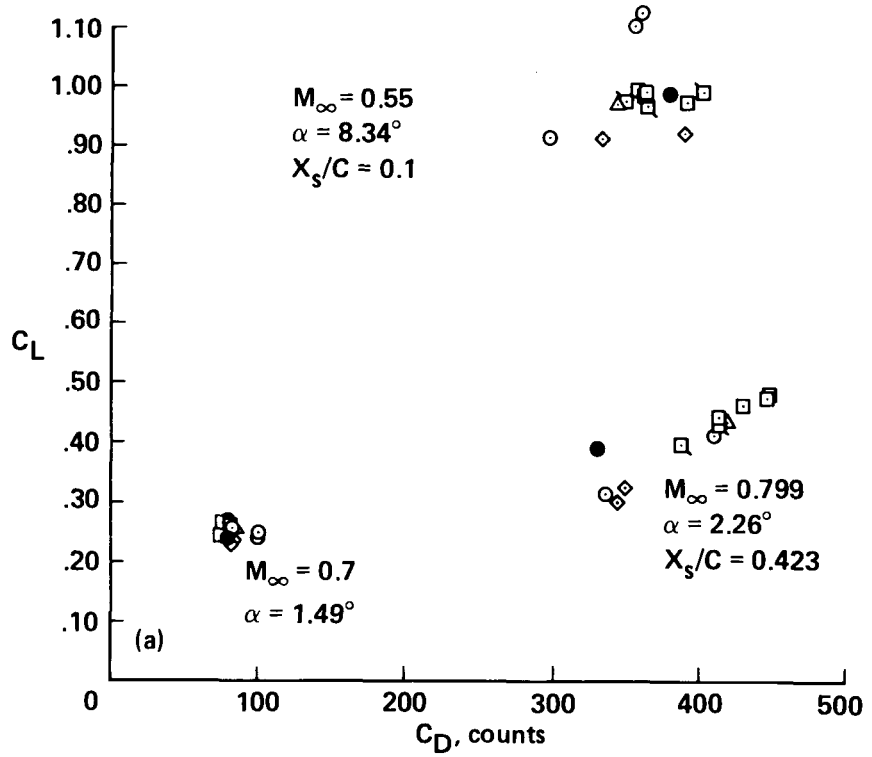

(a) NASA 0012, $Re_c = 9 \times 10^6$.

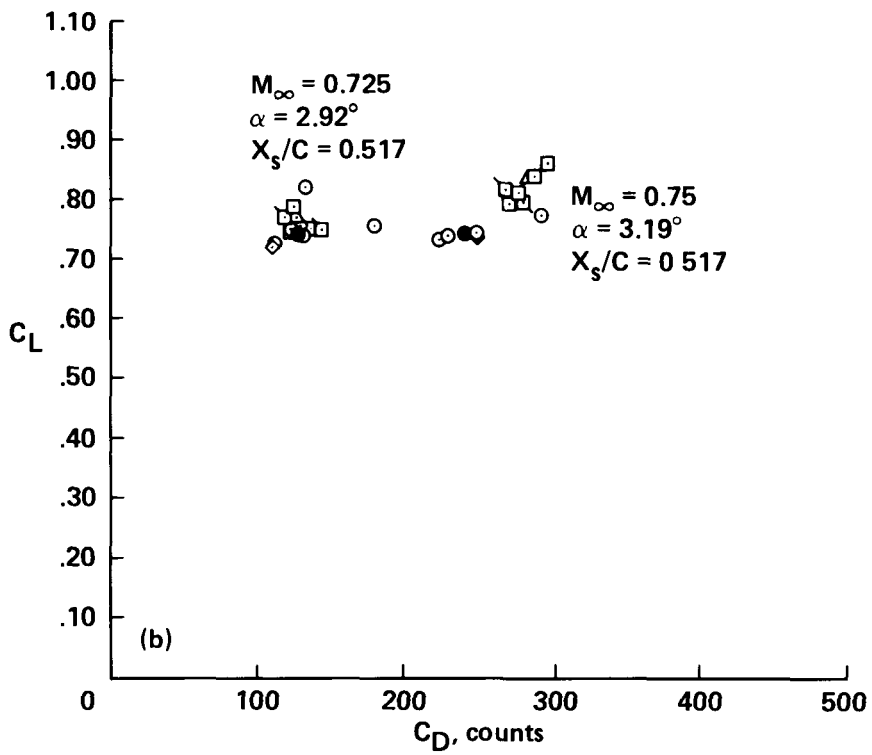

(b) RAE 2822, $Re_c = 6.5 \times 10^6$.

Figure 1.- Comparison of measured and computed force coefficients of transonic airfoils. Symbol legend: experimental data ●; solutions from interactive methods ○; Navier-Stokes solutions with Baldwin-Lomax model □; Cebeci-Smith model □; Johnson-King model ◇; and Coakley-1 model △.

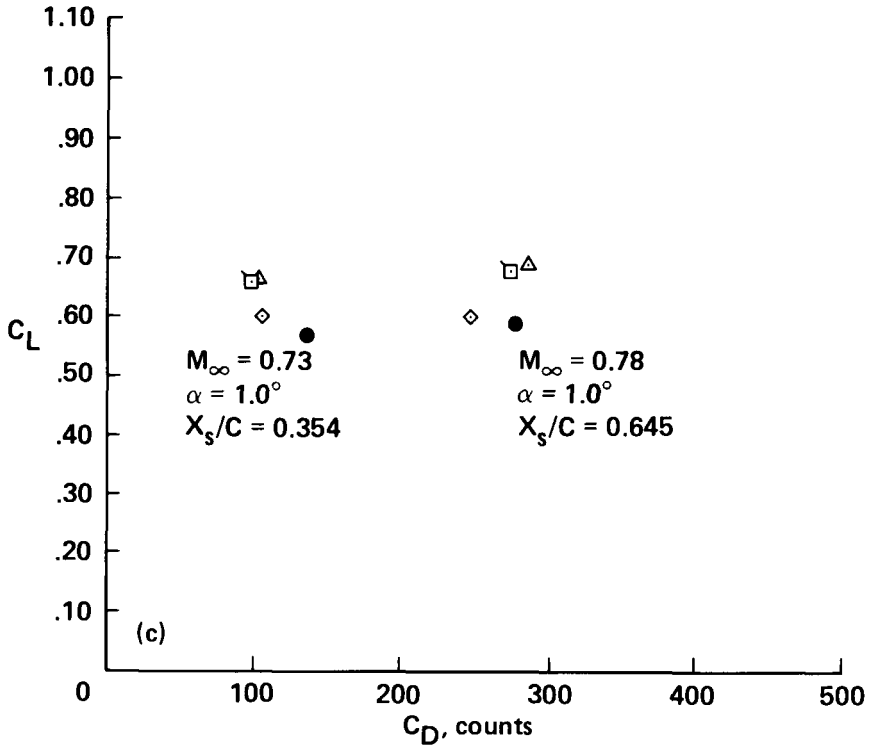

(c) VA-2, $Re_c = 6 \times 10^6$.

Figure 1.- Concluded.

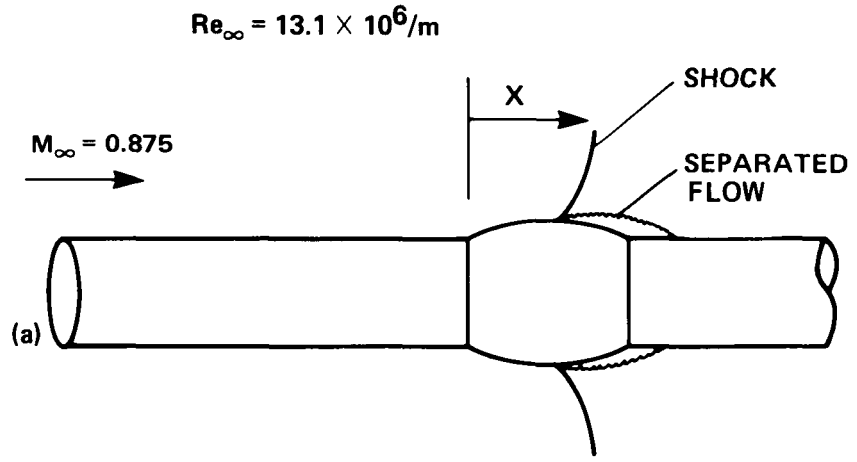

Figure 2.- Schematic diagram of transonic bump model and wind tunnel conditions (ref. 11).

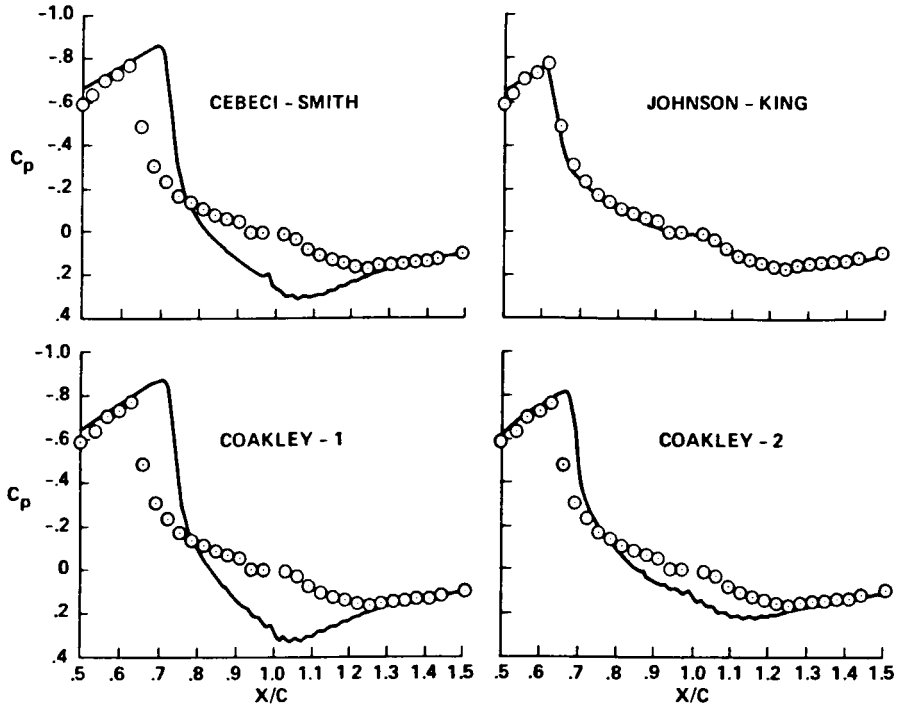

(a) Turbulence models of Cebeci-Smith, Johnson-King, Coakley-1, and Coakley-2.

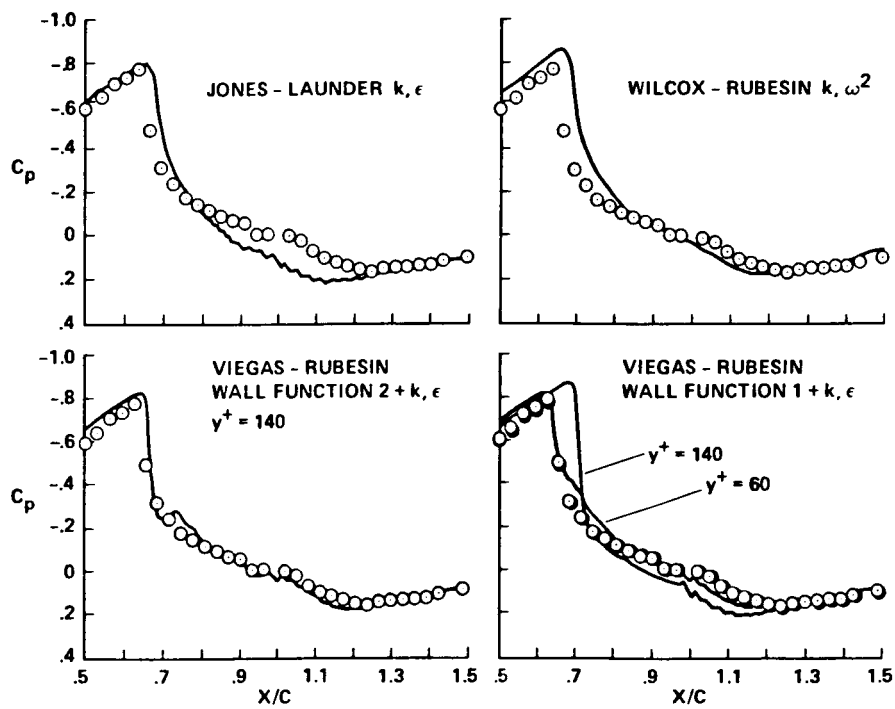

(b) Turbulence models of Jones-Launder, Wilcox-Rubesin, Viegas-Rubesin Wall Functions 1 and 2.

Figure 3.- Pressure distribution over the circular arc bump. The same experimental data, represented by open circles, are repeated in each figure.

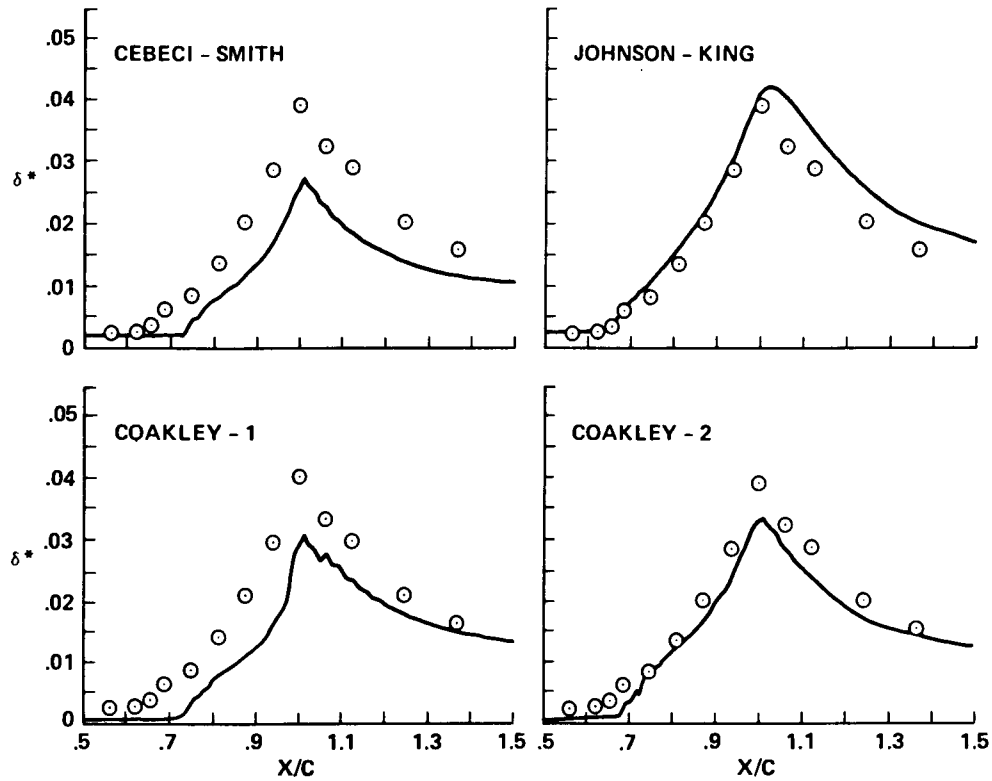

(a) Turbulence models of Cebeci-Smith, Johnson-King, Coakley-1, and Coakley-2.

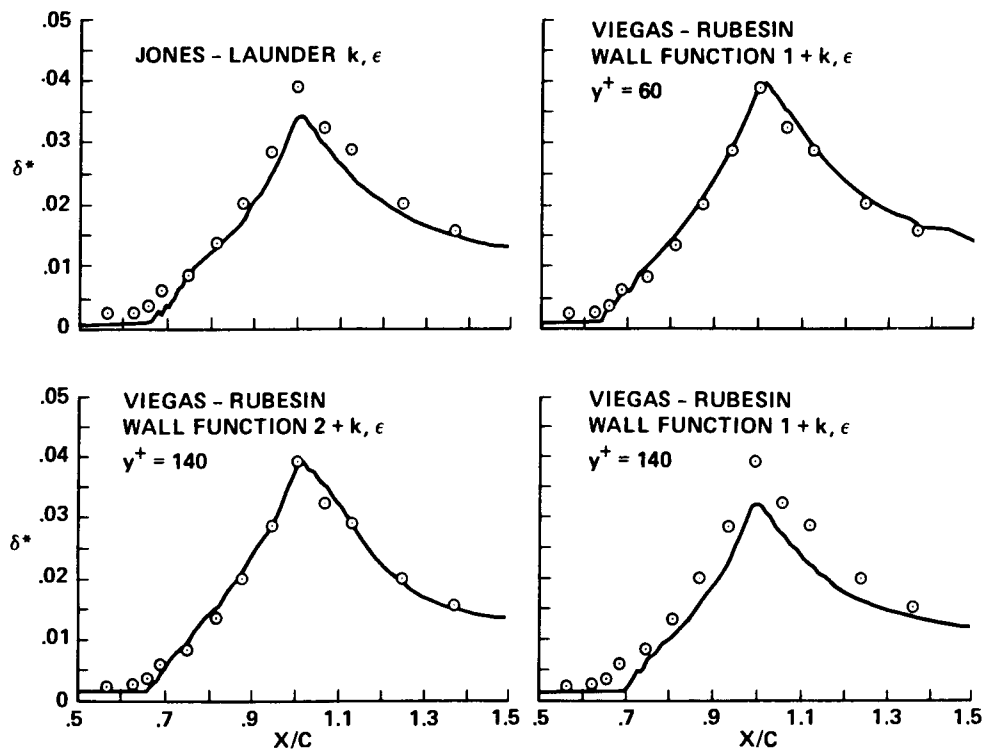

(b) Turbulence models of Jones-Launder, Wilcox-Rubesin, Viegas-Rubesin Wall Functions 1 and 2.

Figure 4.- Displacement thickness over the circular arc bump. The same experimental data, represented by open circles, are repeated in each figure.

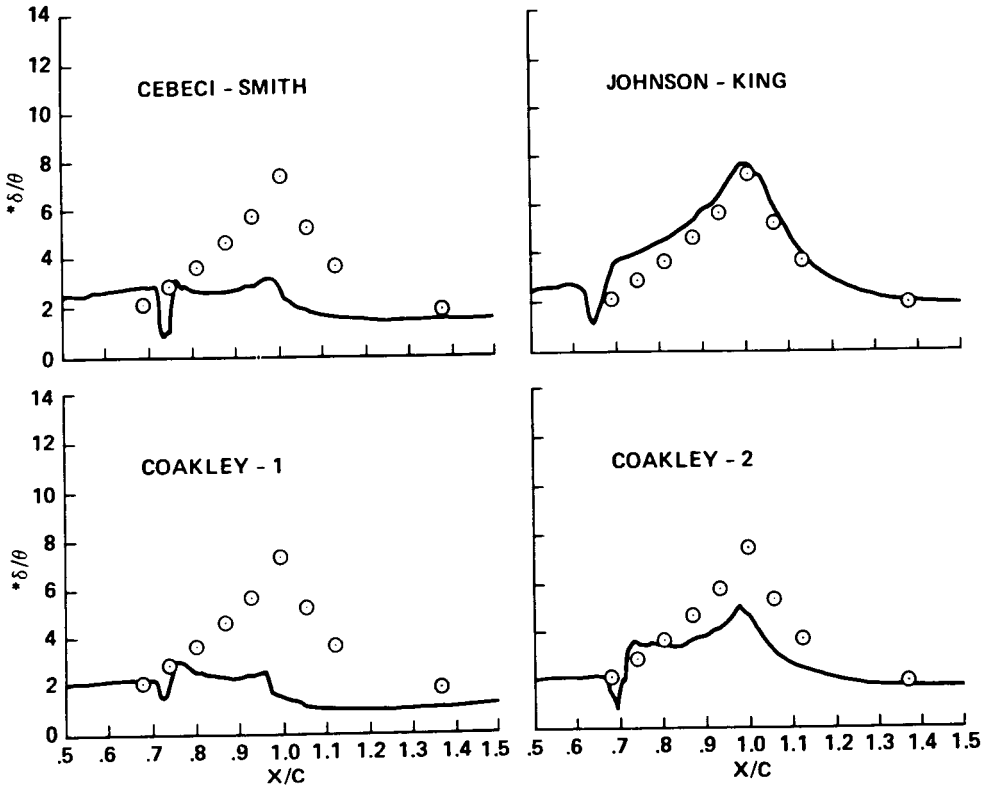

(a) Turbulence models of Cebeci-Smith, Johnson-King, Coakley-1, and Coakley-2.

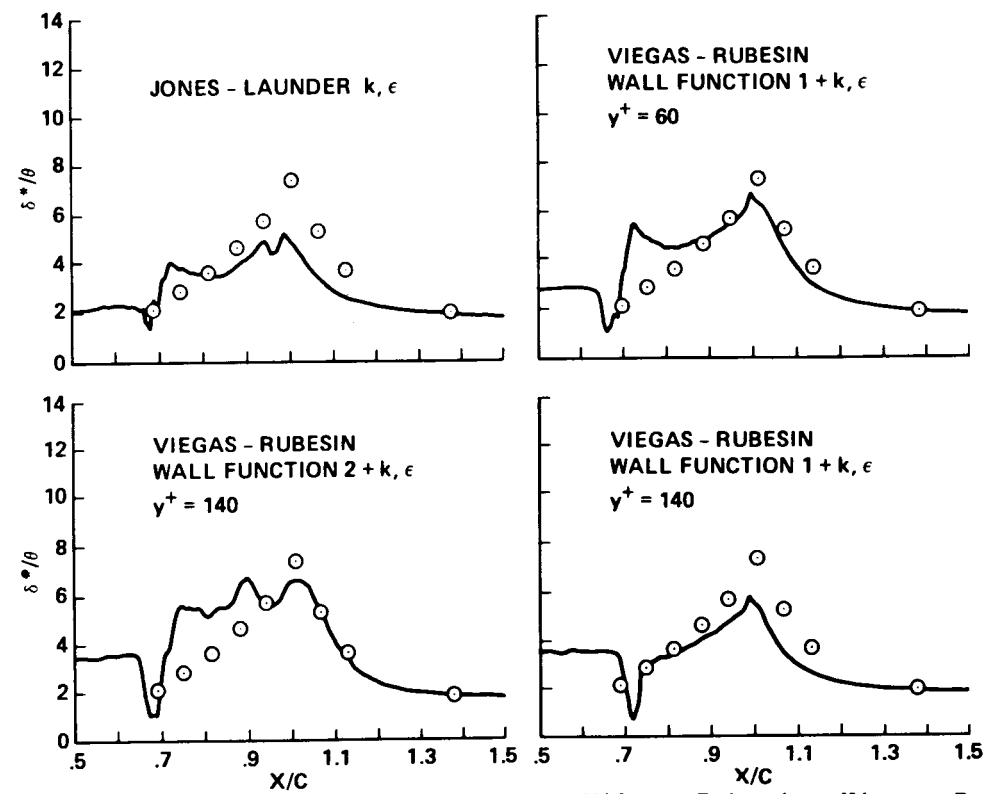

(b) Turbulence models of Jones-Launder, Wilcox-Rubesin, Viegas-Rubesin Wall Functions 1 and 2.

Figure 5.- Shape factor over circular arc bump. The same experimental data, represented by open circles, are repeated in each figure.

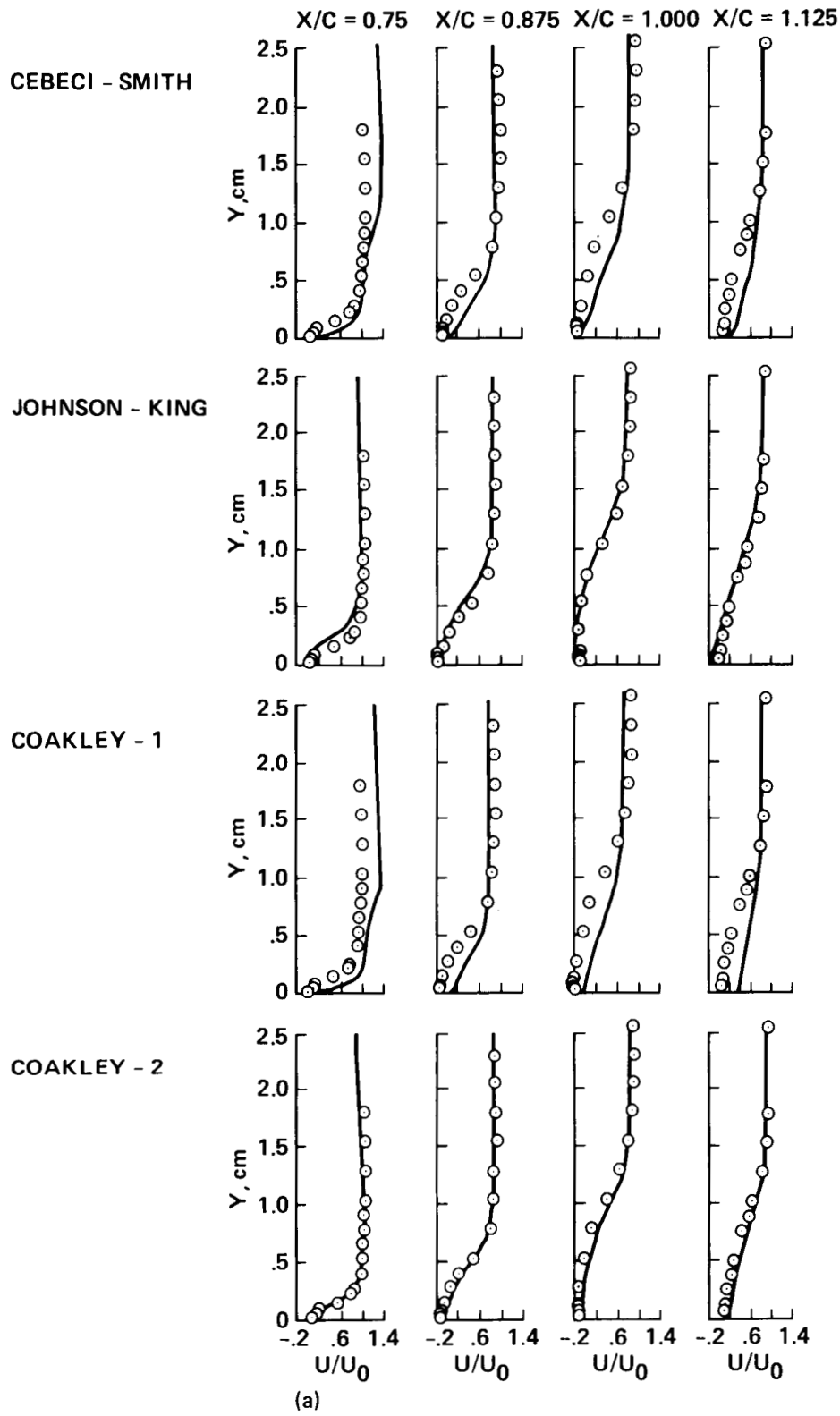

(a) Turbulence models of Cebeci-Smith, Johnson-King, Coakley-1, and Coakley-2.

Figure 6.- Mean velocity profiles over the separation zone on the circular arc bump. The same experimental data, represented by open circles, are repeated in each figure.

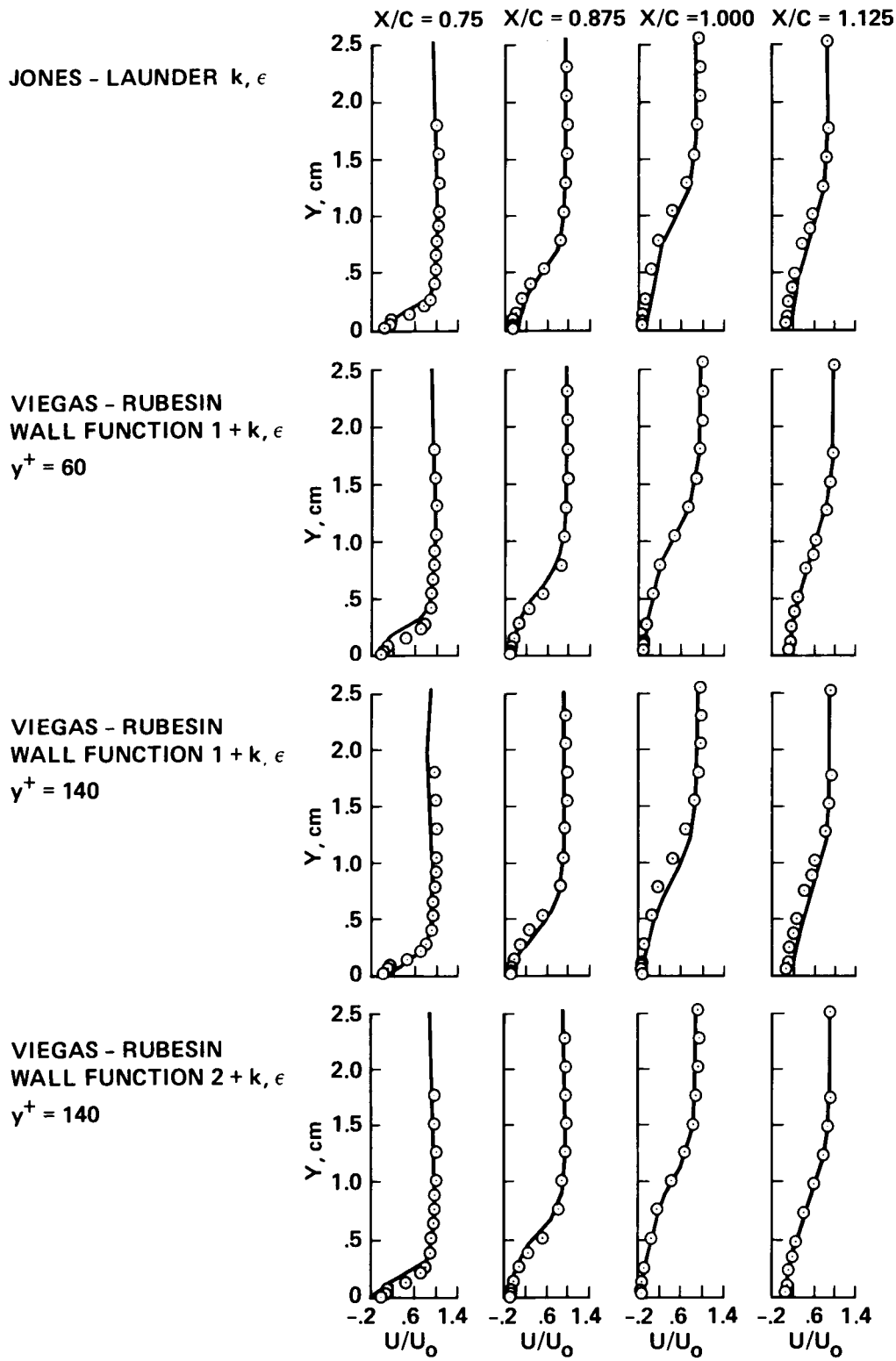

(b) Turbulence models of Jones-Launder, Wilcox-Rubesin, Viegas-Rubesin Wall Functions 1 and 2.

Figure 6.- Concluded.

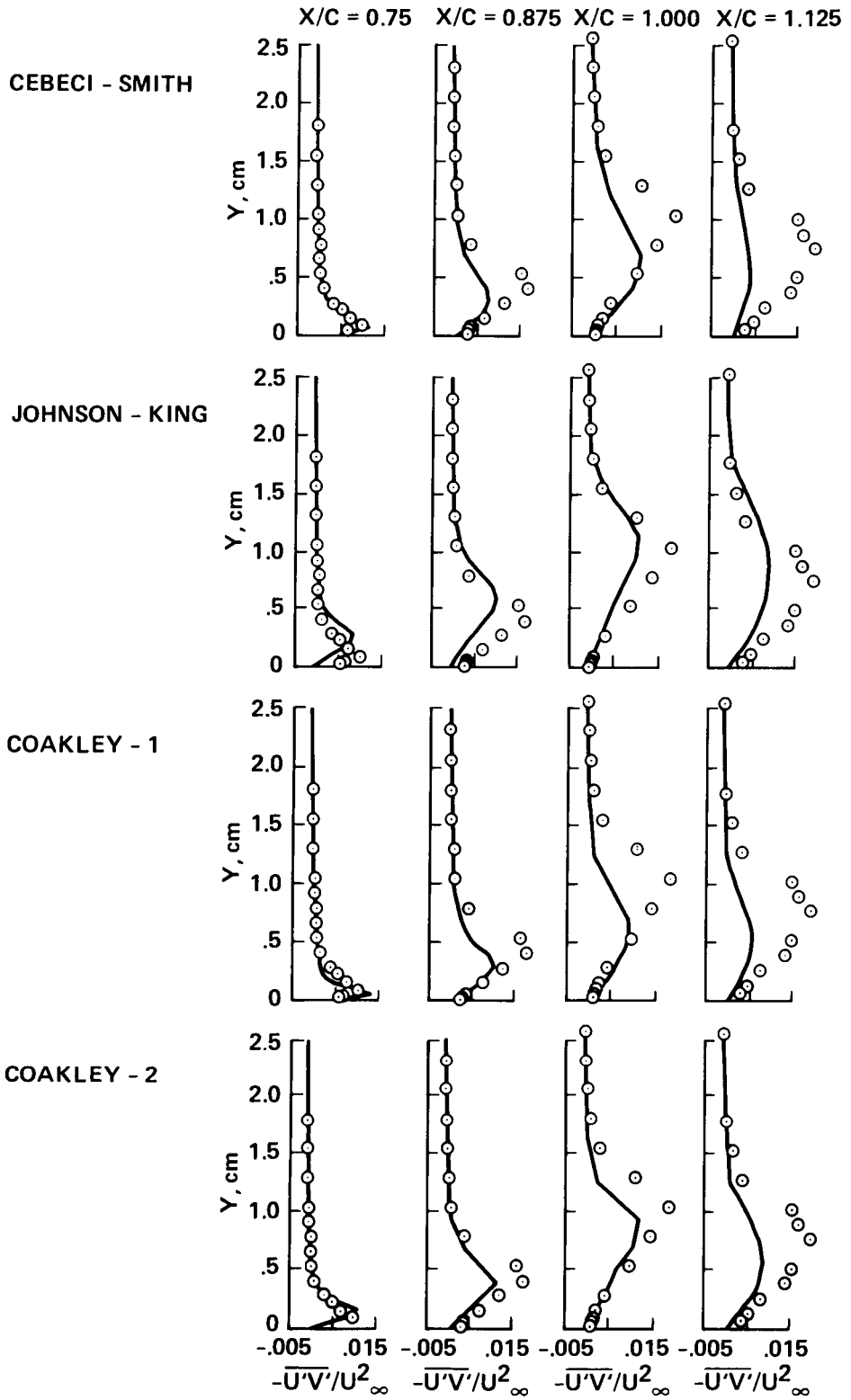

(a) Turbulence models of Cebeci-Smith, Johnson-King, Coakley-1, and Coakley-2.

Figure 7.- Shear stress profiles in the separation zone on the circular arc bump. The same experimental data, represented by open circles, are repeated in each figure.

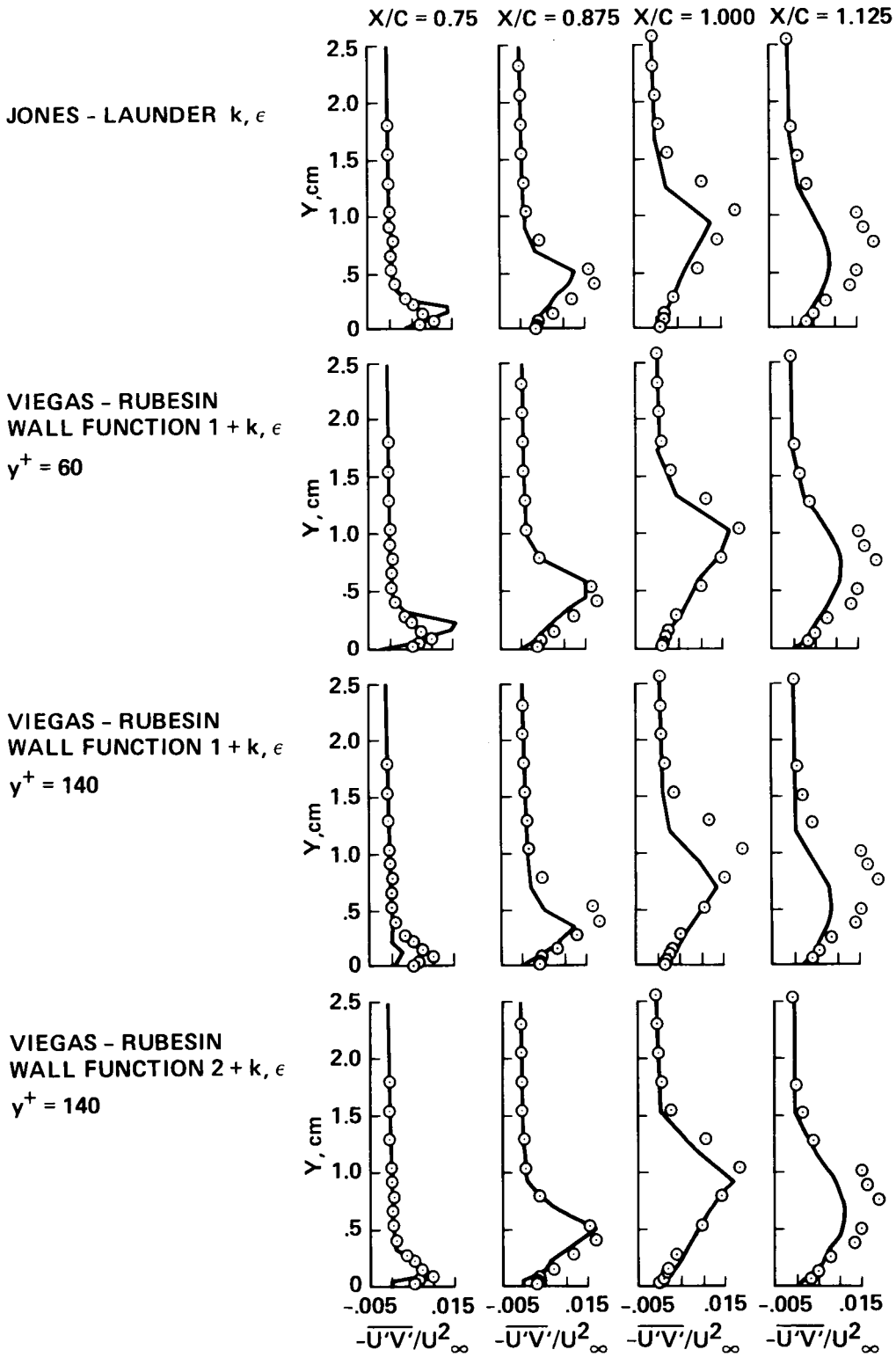

(b) Turbulence models of Jones-Launder, Wilcox-Rubesin, Viegas-Rubesin Wall Functions 1 and 2.

Figure 7.- Concluded.